The Effect of Random Cell Decoupling on Electrogram Morphology near the Percolation Threshold in Microstructural Models of Cardiac Tissue

Marjorie Letitia Hubbard[1], Joshua Xu[1], Craig S Henriquez[1]

[1]Duke University, Durham, NC, USA

Abstract

Random clusters of decoupled cells caused by cell death in diseased cardiac tissue can increase structural heterogeneity and give rise to abnormal patterns of propagation. The objective of this study was to use a 2-D 0.6 cm x 0.6 cm randomly generated model of a ventricular monolayer (LRd membrane model) (dx=dy=10 μm) to study the relationships between the underlying cardiac microstructure, the pattern of wavefront activation, and electrogram morphology as the substrate transitions from well-connected to disconnected. A fraction of individual cells (~100μm x30 μm) between 0 and 0.50 were randomly uncoupled from neighboring cells. Simulated unipolar electrograms were computed at 121 distinct sites at the center of the tissue during longitudinal and transverse propagation. Compared to propagation in the longitudinal direction, conduction block in the transverse direction occurred at a lower percolation threshold (0.44 vs. 0.50) and was associated with a greater fraction of negative asymmetric electrograms. Directional differences in the percolation threshold and electrogram asymmetry were found to be correlated with slow, delayed propagation through isthmuses between decoupled cells. Analysis of electrogram morphology may be useful for identifying regions of tissue that may be vulnerable to long conduction delays and wavefront reentry.

1. Introduction

Structural heterogeneity caused by cell death and scarring in diseased cardiac tissue can give rise to abnormal patterns of propagation [1]. Propagation in cardiac tissue with structural heterogeneity can be characterized using percolation theory, a mathematical model used to describe the probability that there is an open path for a wavefront to propagate through a network with a fraction of disconnected links [2]. When the fraction of disconnected links reaches critical value termed the percolation threshold, wavefront propagation blocks [2]. Previous studies have demonstrated that heterogeneities in source-load mismatch near the onset of conduction block caused by cardiac microstructure can facilitate wavefront breakthrough and reentry [3,4]; however, only a few studies have investigated the impact of these microscale variations in source-load mismatch on electrogram morphology near the percolation threshold in structurally heterogeneous tissue. One two-dimensional computational study using a discrete, heterogeneous model of cardiac tissue has shown that near the percolation threshold, distinct patterns of propagation and block in a localized region of poor coupling can increase vulnerability to reentry [2]. A more recent experimental and computational study of co-cultures of normal and connexin deficient myocytes, representative of a percolating network, has shown that heterogeneous cell decoupling has a nonlinear effect on conduction velocity and that extracellular waveforms show irregular shape as the level of decoupled cells increases [5]. This is consistent with several studies that have also demonstrated that quantitative analysis of features of electrogram morphology such as amplitude, asymmetry, and fractionation may be useful for discriminating the degree and pattern of structural heterogeneity [1,6,7]. The objective of this study was to use 2-D computer models of adult monolayers to investigate quantitatively the effect of increasing the fraction of decoupled cells on wavefront propagation and electrogram morphology near the percolation threshold.

2. Methods

2.1. Tissue models

Two-dimensional computer models (0.60cmx0.60cm) of ventricular monolayers that incorporate discrete cells, with uniformly distributed gap junctions (g_j), were randomly generated using methods previously described [8]. The spatial discretization was dx=10 μm, dy=10 μm, and the individual myocytes were an average of 100 μm in length and 30 μm in width. The gap junction conductivity was set to 0.30 μS/cm^2 and the intracellular resistivity was set to 150 Ω-cm. A fraction of individual

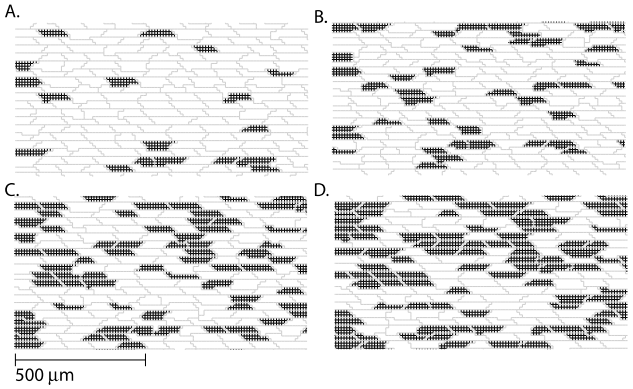

Figure 1. Microstructural models with different fractions (*F*) of decoupled cells. (A) *F*=0.10 (B) *F*=0.20 (C) *F*=0.30 (D) *F*=0.40. Decoupled cells are shown in dark gray.

cells (*F*) between 0 and 0.50 were randomly decoupled by removing gap junctions from the entire boundary of single cells (Fig. 1). For each case, three randomly generated inhomogeneous tissue models representing different realizations of the same microstructure statistics (cell shape, size, coupling, fraction of decoupling) were created in order to test the sensitivity of the results to random changes in tissue architecture. Equivalent continuous models (dx=10 µm, dy=10 µm) with clusters of decoupled cells but no discrete gap junctions were created by adjusting the uniform resistivity of the continuous model to match the longitudinal and transverse conduction velocities measured in a 0.60 cm x 0.60 cm discrete tissue model with no cell decoupling. The size and shapes of the obstacles in the equivalent continuous models were matched to those in the discrete models.

2.2. Simulation protocol

All simulations used the CardioWave software platform[9]. A modified LRD model of guinea pig ventricular tissue was used to simulate the ionic properties. The tissue was stimulated with longitudinal plane waves along the left axis or transverse plane waves along the bottom axis. A semi-implicit scheme with a conjugate gradient solver was used to solve the system of equations. The time step was kept constant at 5 µs, output data were recorded every 10 µs, and the data for the activation maps were recorded at a minimum of every 100 µs. Conduction velocity for tissues with a decoupling fraction between 0 and 0.40 was calculated by taking a linear regression of the activation times.

2.3. Unipolar electrograms

Simulated unipolar electrograms were computed at 121 distinct sites throughout the tissue from an 11x11 rectangular grid of idealized point electrodes, with an interelectrode spacing of 200 µm. Electrogram morphology was characterized by the number of peak deflections and amplitude (A, Eq. 1) and asymmetry (a, Eq. 2) of the signals defined as follows [6]:

(Eq. 1) $A = R + S$ (Eq. 2) $a = \frac{R - S}{R + S}$

where R and S are the absolute value of the maximum and minimum of the electrogram voltage.

The electrogram amplitude was scaled such that the average peak-to-peak amplitude in the control tissues during longitudinal propagation was equal to 10 mV. The deflection peaks were determined such that no peak values smaller than 5% of the maximum peak value in each tissue model were included. No distinction was made to account for variation in the slopes of the deflection peaks.

3. Results

3.1. Longitudinal propagation

Along the longitudinal axis, conduction velocity slowed from 50.4 cm/s to 12 cm/s as the fraction of decoupled cells increased from 0 to 0.45, and wavefront propagation eventually blocked at a longitudinal percolation threshold of 0.50. Near the percolation

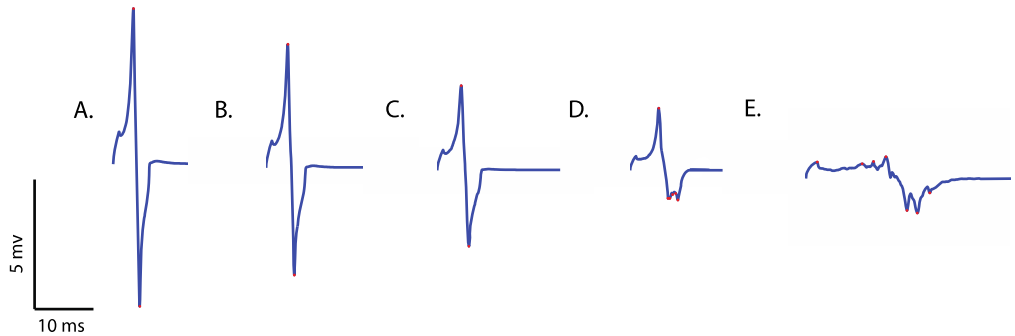

Figure 2. Example electrograms measured during longitudinal propagation in tissue with different fractions (*F*) of cell decoupling. (A) *F*=0 (B) *F*=0.10 (C) *F*=0.20 (D) *F*=0.30 (E) *F*=0.40.

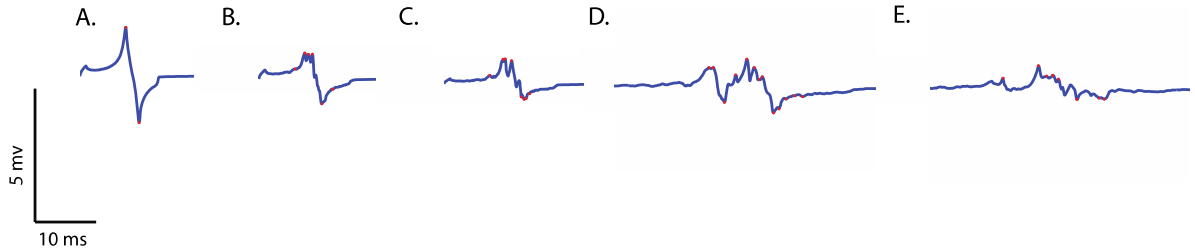

Figure 3. Example electrograms measured during transverse propagation in tissue with different fractions (*F*) of cell decoupling. (A) *F*=0 (B) *F*=0.10 (C) *F*=0.20 (D) *F*=0.30 (F) *F*=0.40

threshold, the pattern of wavefront propagation shifted from a plane wave to discrete pathways of anterograde and retrograde conduction as the wave meandered around clusters of decoupled cells.

In control tissue with no cell decoupling, the electrogram amplitude was 10 ± 0.2 mV and asymmetry was 0.07 ± 0.03. As the fraction of decoupled cells increased from 0 to 0.40, the variation in electrogram asymmetry increased, and the fraction of electrograms with positive asymmetry remained greater than 0.50. Near a decoupling fraction of 0.30, the unipolar electrograms began to exhibit fractionation that was correlated with the wavefront microcollisions. The average number of deflections increased from 2 to 8.59±3.74 as the fraction of decoupled cells approached the longitudinal percolation threshold of 0.50. Examples of electrograms measured during longitudinal propagation in tissue with different fractions of decoupling are shown in Fig. 2.

In general, there was no significant difference between the global percolation threshold or amplitude and degree

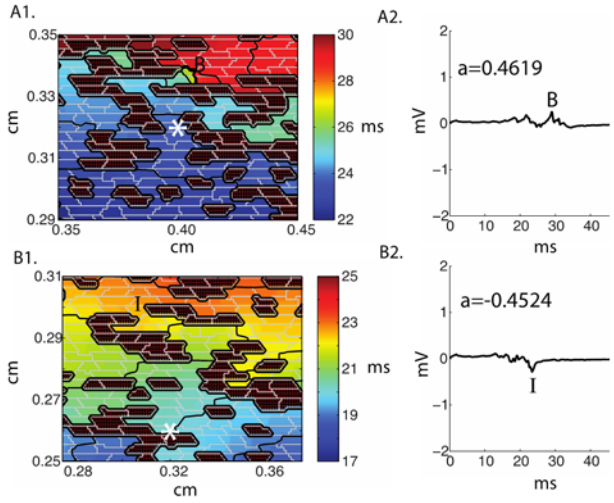

Figure 4. Activation maps (ischchrones shown every 1 ms) and electrograms measured at sites of maximum and minimum electrogram asymmetry during transverse propagation in tissue with *F*=0.30. Electrode locations are indicated with a star. B indicates site of conduction block and microcollision. I indicates site of isthmus.

of positive electrogram asymmetry measured in corresponding realizations of microstructural and equivalent continuous models during longitudinal propagation. Close to the percolation threshold (F=0.45), however, there were localized differences in the pattern of propagation observed during longitudinal propagation. At the longitudinal percolation threshold, the discrete microstructural model exhibited a higher degree of localized conduction block and wavefront collision, which manifested as a slightly higher fraction of positive asymmetric electrograms (0.89) compared to the continuous model (0.77).

3.2. Transverse propagation

Along the transverse axis, conduction velocity slowed from 24.1 cm/s to 6.40 cm/s as the fraction of decoupled cells increased from 0 to 0.40, and wavefront propagation eventually blocked at a transverse percolation threshold of 0.44. Near the percolation threshold, the pattern of wavefront propagation shifted from a plane wave to alternating pathways of transverse and longitudinal conduction.

In control tissue with no cell decoupling, the electrogram amplitude was 3.09±0.05 mV and asymmetry was 0.0485±0.024. As the fraction of decoupled cells increased from 0.10 to 0.40, the electrogram amplitude decreased from 2.21±0.21 mV to 0.7218±0.15. As the fraction of decoupled cells increased from 0 to 0.40, the variation in electrogram asymmetry increased, the electrogram asymmetry became negative (-0.2122±0.31), and the fraction of negative asymmetric electrograms reached as low as 0.2810. The increase in the fraction of negative asymmetric electrograms was more pronounced during transverse propagation compared to longitudinal propagation and occurred at lower decoupling fractions.

In contrast to propagation in the longitudinal direction, fractionation appeared during transverse propagation at a decoupling fraction of 0.10 and was correlated with small collisions at the microscale as the wave meandered around small clusters of decoupled cells. The number of deflections increased from 2 to 9.84±2.56 as the fraction of decoupled cells increased from 0.10 to 0.30 and

decreased slightly as to 7.98±2.55 as the tissue approached the longitudinal percolation threshold of 0.44, suggesting that the degree of fractionation was correlated with both the zig-zag pattern of decoupled cells through narrow isthmuses as well as the dimensions of the decoupled cluster. Examples of electrograms measured during transverse propagation in tissue with different fractions of decoupling are shown in Fig. 3.

Activation maps taken at sites of minimum and maximum asymmetry across the tissue during transverse propagation suggested that a localized site of maximum asymmetry shown in Fig. 4A2 was associated with wavefront-wavefront collisions caused by conduction block at narrow isthmuses openings, while a localized site of maximum negative asymmetry shown in Fig. 4B2 was associated with source-load mismatch caused by propagation out of narrow isthmuses into a larger load**.**

4. Conclusions

Analysis of electrogram morphology may be useful for identifying regions of tissue near the percolation threshold that may be vulnerable to long conduction delays and wavefront reentry. Although microstructural variations in the different realizations of the tissue models resulted in varying electrogram morphologies as the fraction of decoupled cells increased, several characteristics were observed. Near the percolation threshold for longitudinal propagation, electrograms exhibited low amplitude, a greater fraction of negative asymmetric electrograms, and increased number of deflections. During transverse propagation, electrograms also exhibited low amplitude, a greater fraction of negative asymmetric signals, and increased number of deflections but at a lower threshold compared to the longitudinal direction.

The directional differences in the percolation threshold and electrogram morphology may be correlated with the differences in the pattern of cell arrangement and cell decoupling in the longitudinal and transverse directions. Electrogram morphology is determined by the interplay between wavefront collisions, which increase the number of peak deflections and are associated with positive asymmetry and delayed propagation through the openings of isthmuses, which are associated with negative asymmetry. Wavefront collisions can be caused by propagation around clusters of obstacles or by localized block at sites of source-load mismatch, both of which cause electrograms with positive asymmetry. In this study, the clusters of decoupled cells also tend to have a greater length than width, and previous studies have shown that the length of the obstacle influences positive electrogram asymmetry [6]. In the transverse direction, conduction is slower because of the cell geometry and isthmuses appear at lower levels of decoupling than in the longitudinal direction, leading to a lower percolation threshold and a greater fraction of negative asymmetric electrograms.

This study did not investigate the effect of electrode size on fractionation. In a study of wavefront propagation in a fibrotic tissue model, Jacquemet et. al. found that increasing the size of the electrode results in spatial averaging that decreases the amplitude of the unipolar electrogram and decreases the number of sharp deflections [6]. Consequently, the size of the electrode may have a strong influence on directional differences in electrogram morphology. Future studies will systematically investigate the effect of isthmus size, the pattern of structural heterogeneity, and electrode size using quantitative measures of electrogram morphology such as asymmetry, the degree of fractionation and more robust measures of signal analysis.

References

[1] Campos FO, Wiener T, et. al. Electroanatomical characterization of atrial microfibrosis in a histologically detailed computer model. IEEE Trans Biomed Eng 2013; 60: 2339-2349.

[2] Alonso S, Bar M. Reentry near the percolation threshold in a heterogeneous discrete model for cardiac tissue. Phys Rev Lett 2013; 110: 5.

[3] Hubbard ML, Henriquez CS. Microscopic variations in interstitial and intracellular structure modulate conduction delays and block in cardiac tissue with source-load mismatch. Europace 2012; 14: v3-v9.

[4] Hubbard ML, Henriquez CS. A microstructural model of reentry arising from focal breakthrough at sites of source-load mismatch in a central region of slow conduction. American Journal of Physiology - Heart and Circulatory Physiology 2014; 306: H1341-H1352.

[5] Prudat Y, Kucera JP. Nonlinear behaviour of conduction and block in cardiac tissue with heterogeneous expression of connexin 43. J Mol Cell Card 2014; 76C:46-54.

[6] Jacquemet V, Henriquez CS. Genesis of complex fractionated atrial electrograms in zones of slow conduction: A computer model of microfibrosis. Heart Rhythm 2009; 6: 803-810.

[7] Ellis WS, Auslander DM, Lesh MD. Fractionated Electrograms From a Computer Model of Heterogeneously Uncoupled Anisotropic Ventricular Myocardium. Circ 1995; 92: 1619-1626.

[8] Hubbard ML, Ying W, Henriquez CS. Effect of gap junction distribution on impulse propagation in a monolayer of myocytes: a model study. Europace 2007; 9: vi20-28.

[9] Pormann J. A modular simulation system for the bidomain equations. PhD Thesis. Duke University Department of Electrical and Computer Engineering, 1999.

Address for correspondence.
Marjorie Letitia Hubbard
Duke University
136 Hudson Hall
Durham, NC 27704
mlh23@duke.edu